

Stabilization of beam heated plasmas by beam modulation

L. Einkemmer¹*Universität Innsbruck, A-6020 Innsbruck, Austria*

(*Electronic mail: lukas.einkemmer@uibk.ac.at)

(Dated: 26 November 2024)

A constant intensity beam that propagates into a stationary plasma results in a bump-on-tail feature in velocity space. This results in an instability that transfers kinetic energy from the plasma to the electric field. We show that there are intensity profiles for the beam (found by numerical optimization) that can largely suppress this instability and drive the system into a state that, after the beam has been switched off, remains stable over long times. The modulated beam intensity requires no feedback, i.e. no knowledge of the physical system during time evolution is required, and the frequency of the modulation scales approximately inversely with system size, which is particularly favorable for large plasma systems. We also show that the results obtained are robust in the sense that perturbations, e.g. deviation from the optimized beam profiles, can be tolerated without losing the ability to suppress the instability.

I. INTRODUCTION

A particle beam that propagates into a stationary plasma can drive a microinstability. Due to the additional peak (the beam) in the velocity distribution that is superimposed on the Maxwellian equilibrium, this is called the bump-on-tail instability. The instability is driven by the unfavorable slope of the velocity distribution, which allows the transfer of energy from fast particles to the electric field. The electric field then grows exponentially until nonlinear effects become strong enough to lead to saturation.

The bump-on-tail instability has been studied extensively (see, e.g.,¹⁻⁴). It is relevant for fusion plasmas as beam heating (the injection of high energy particles to heat a plasma; see, e.g.,⁵) and ion cyclotron heating (the heating of the plasma by absorption of electromagnetic radiation) creates bump-on-tail features (see, e.g.,²). Bump-on-tail features from plasma heating as well as runaway electrons can destabilize Alfvén waves⁶ and potentially degrade reactor performance^{4,7}. For example, in⁴ it has been demonstrated that simple beam modulation (turning the beam on and off with a certain frequency) can significantly effect the ion transport even if the same amount of heating is injected into the plasma. It has also been pointed out⁸ that the bump-on-tail instability plays a significant role in plasma thrusters (such as in the variable specific impulse magnetoplasma rocket – VASIMR).

A natural question then is whether a sufficiently strong beam necessarily leads to an instability or if some type of control can be achieved. Control theory is well established, but such schemes usually require feedback that is obtained by taking measurements from the system under investigation. Based on these measurements certain actions are then taken to stabilize the system or achieve some other goal^{9,10}. The classic example is the inverted pendulum stabilized by a PID controller. However, feedback, poses a severe constraint for kinetic instabilities that often take place on very fast time scales (say the inverse of the plasma frequency or the Alfvén time). Thus, such an approach would require that data acquisition, data processing, and the subsequent modification of the control variable (say the intensity of the beam) is fast enough to follow the plasma dynamics. In most situations this is not feasible. In addition, beam-plasma instabilities are inher-

ently driven by non-Maxwellian velocity features, for which in most cases only limited information can be obtained experimentally.

While feedback based control might be infeasible for microinstabilities, it has been observed that modulating the beam intensity with a fixed frequency can reduce the severity of the bump-on-tail instability. In¹¹ it was experimentally demonstrated that modulating an electron beam close to the natural oscillation frequency of the system reduces the electric field strength observed during the instability. Later this problem was also studied by computer simulations. In¹² the authors considered the nonlinear coupling of a relatively small number of modes finding similar results. In¹³ a related problem is investigated where the velocity (not the intensity) of the beam is modulated. Neglecting thermal effects, the authors develop a linear theory that shows that varying the velocity of the beam sinusoidally reduces the growth rate of the instability (the frequency of modulation is close to the plasma frequency). Similar observation, i.e. that a sinusoidal modulation can have a stabilizing effect, have also been made in the context of inertial confinement fusion, where it is desirable to suppress or delay a Rayleigh–Taylor instability. The interpretation given in¹⁴ is that an instability can be counteracted if the phase is known. While measuring the phase of a naturally developing instability is difficult in practice, a modulated beam can define the phase of the perturbation and thus the instability can be counteracted.

The problem of suppressing a two-stream/bump-on-tail instability with a time and space dependent external electric field as control has also been considered recently^{15,16}. The theoretical results obtained indicate that the instability can be completely suppressed without feedback if the initial state is known. The issue, however, is that injecting an arbitrary electric field into a plasma is difficult in practice and that the initial deviation from equilibrium needs to be precisely known. Nevertheless, it raises the question what the ultimate limit of control is in situations where the control is less direct, such as the case of beam modulation that we consider here.

In this paper our goal is to study a simple kinetic model of a stationary plasma in which a (possibly modulated) beam is injected. The question is whether the associated bump-on-tail instability can be suppressed or reduced without requiring

feedback and, if so, how fast this modulation needs to be in order to be successful. Our goal is also to find beam profiles by numerical optimization that are more effective than modulating the beam in a sinusoidal manner.

II. MODEL

For the electron dynamics we consider the one dimensional non-dimensionalized Vlasov–Poisson equation

$$\partial_t f + v \partial_x f - E \partial_v f = S, \quad (1)$$

where $f(t, x, v)$ is the electron density and the beam is modeled by a source term

$$S(t, x, v) = I(t) \frac{1}{\sqrt{2\pi}\sigma} \exp\left(\frac{-(x-x_0)^2}{2\sigma^2}\right) \cdot \frac{1}{\sqrt{2\pi}v_{th,b}} \exp\left(\frac{-(v-v_b)^2}{2v_{th,b}^2}\right), \quad (2)$$

where $I(t)$ is the modulated beam amplitude. We assume that the beam has a Gaussian profile in space (centered at the middle of the domain x_0 ; the spatial extent of the beam is σ) and is Maxwellian in velocity (with average beam velocity v_b and thermal velocity of the beam $v_{th,b}$). We assume that the ions form a homogeneous neutralizing background. Thus the electric field is given by $E = -\partial_x \phi$ with the potential ϕ satisfying $-\partial_{xx} \phi = \rho$. The charge density ρ is given by $\rho = \int f d(x, v) - \int f dv$. We use a domain of size L and periodic boundary conditions. Note that as the beam adds particles to the system the number density is time dependent and is given by $\int f(t, x, v) d(x, v) = 1 + \int_0^t I(s) ds$. In principle we could also modulate the spatial extent σ , the beam velocity v_b , and the thermal speed $v_{th,b}$, but to keep the control relatively straightforward we will not do so here. All units of time and velocity are normalized to the plasma frequency (ω_p) and thermal velocity (v_{th}) of the bulk plasma (i.e. the thermal velocity of the initial electron distribution), respectively. This implies units of Debye length (λ_D) for all spatial variables. The electric field is normalized such that no additional factor appears in the Poisson equation for the potential. More specifically, in SI units we have $E = E_{SI}/E_{ref}$ with $E_{ref} = m\lambda_D\omega_p^2/e$, where m is the electron mass and e the unit charge.

The model outlined is a fundamental model in plasma physics that has been studied extensively both using linear theory and (usually nonlinear) computer simulations. It is well known that adding a second peak (the bump on the tail) to a Maxwellian velocity distribution, above a certain threshold intensity, results in a plasma instability. Theoretically this can be analyzed either by considering a separate fluid description of the bulk plasma and the beam¹⁷ or, more accurately, by deriving the dispersion relation within a fully kinetic description¹⁸. In the latter case, the Penrose criterion¹⁹ is not satisfied and the bump-on-tail configuration is unstable. The associated dispersion relation can be solved to obtain the

(linear) growth rate of the instability. The linear regime is accompanied by an exponential increase of the electric energy, i.e. kinetic energy of the plasma is transferred to the electric field. Eventually the system becomes strongly nonlinear and the amplitude of the electric field saturates; the latter is not captured by linear theory. The described analysis is concerned with a static situation. That is, it is assumed that, in some way, the system is prepared in a state where a bump-on-tail feature is present. The plasma system is then allowed to evolve on its own without further intervention. Here, in contrast, we are interested in a dynamic situation. That is, the plasma is initially a current free and spatially homogeneous Maxwellian and the beam, modeled by the source term S , dynamically creates the bump-on-tail feature and triggers the instability. This setup is illustrated in Figure 1.

In our model of the beam we have four parameters: the beam amplitude I , the spatial extent σ , the beam velocity v_b , and the beam thermal velocity $v_{th,b}$. Note that the thermal velocity has a significant influence. Increasing the thermal velocity such that it is comparable to v_b softens the bump-on-tail feature and makes the system more stable. Thus, we will restrict $v_{th,b}$ to lie between 0.2 and 0.6. The position at which the beam enters the plasma x_0 in our model just corresponds to a shift of the x coordinates and is thus not relevant. The beam velocity v_b determines how much energy is added to the system (for a given beam strength). We thus fix the total energy that is added to the system by mandating that $v_b = 3.5$ and $\int_0^{t_b} I(t) dt = I_0 t_b$, where $I_0 = 0.05$ and t_b is the duration during which the beam is switched on. The goal is then to find $I(t)$, σ , and $v_{th,b}$ such that the bump-on-tail instability is suppressed.

III. RESULTS FOR SINUSOIDAL BEAM PROFILES

First we consider the case of a sinusoidal beam profile $I(t) = I_0 + b_1 \sin(\omega t)$, $I_0 = 0.05$, for $t \leq t_b$ and fixed beam temperature ($v_{th,b} = 0.5$). We consider three configurations that correspond to three different plasma sizes. Specifically, we choose the length of the spatial domain as $L = 4\pi$, $L = 16\pi$, and $L = 64\pi$. The rationale here is that ultimately we are interested in plasmas systems that are large compared to the Debye length. Thus, we want to study how the control schemes (especially the driving frequency, but also the beam width) scales with systems size, as this dictates how fast the beam has to be modulated and how tightly it needs to be focused to achieve the desired effect. The beam width is chosen as $\sigma = 0.2$, $\sigma = 0.8$, $\sigma = 3.2$ for the three configurations respectively; i.e. the beam width in this section is held fixed (for each configuration) and scales proportional with system size. To make the configurations comparable, we choose $t_b = 25$, 100, and 400, respectively. This corresponds to roughly a doubling of the total energy contained in the plasma system after the beam has been switched off and an increase of the particle number by roughly 10%.

In the present setup there are two parameters, the frequency ω and the corresponding amplitude b_1 . The chosen figure of merit, which we use in all numerical simulations in this work,

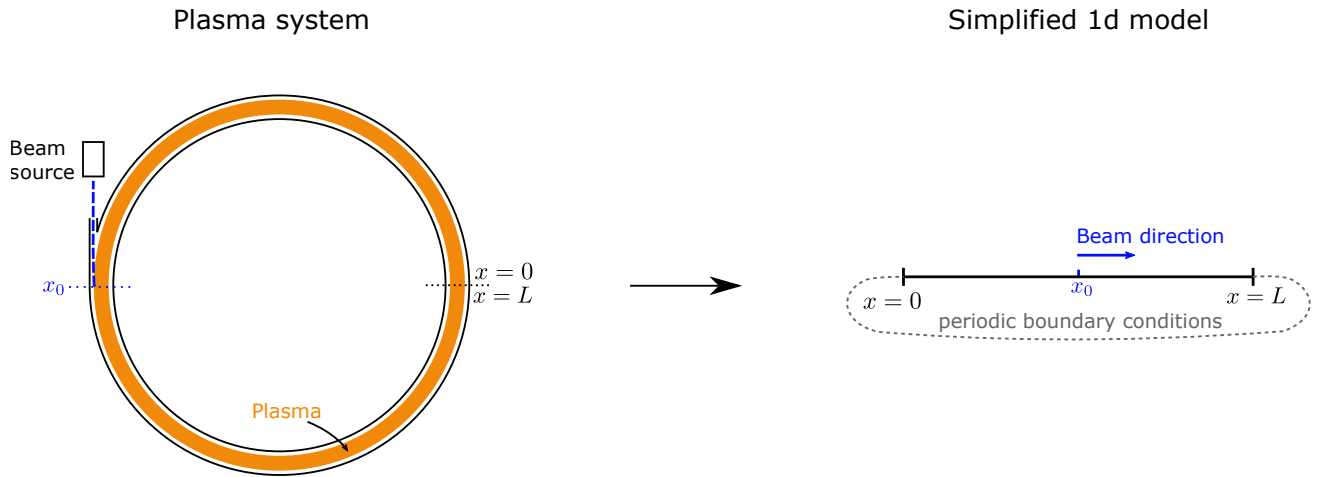


FIG. 1. We consider a plasma system into which a beam is injected. The simplified 1d model used in this study (shown on the right) consists of a domain of length L with periodic boundary conditions. The beam is injected at position x_0 with velocity $v_b > 0$. This can be considered as an idealized version of a toroidal plasma system (as shown on the left) or alternatively a setup similar to¹¹, where a beam is reflected at the end of a vessel that encloses the plasma.

is the time integrated total electric energy, i.e.

$$\text{FOM}[E] = \frac{1}{2} \int_0^{t_f} \int_0^L E^2(t, x) dx dt, \quad (3)$$

where $t_f = 150$ for the small system size and $t_f = 2t_b$ in the other two cases. For the small system size a time longer than $2t_b$ is required such that the instability can fully develop (as the beam is only switched on for a relatively short duration). All results plotted are normalized to the case where the beam is not modulated (i.e., $b_1 = 0$). Thus, we measure the severity of the instability by how much kinetic energy is transferred to the field. If no beam is injected into the plasma the figure of merit is 0 (no instability) and if no modulation is performed the figure of merit is 1. A smaller figure of merit thus corresponds to a larger reduction of the severity of the instability.

We note that in the sense of linear theory, an instability is primarily characterized by its growth rate. Our goal here is not necessarily to reduce this growth rate, but to (a) reduce the electric field strength at which the instability saturates and (b) to obtain a state, after the beam has been switched off, where the electric field is as small as possible (in order to facilitate heating the plasma by the available kinetic energy). The chosen figure of merits represents a compromise between the two.

As can be clearly observed from Figure 2, already a sinusoidal beam, if an appropriate frequency and amplitude is selected, can yield a reduction in the severity of the instability by between 56-78%. In Figure 2c we consider the simulation with the optimal frequency and amplitude for the sinusoidally modulated beam in more detail. We observe that the reduction in the severity of the instability is not merely a transient phenomenon, but persists after the beam has been switched off. In fact, the long time behavior is excellent showing a reduction of the electric energy by approximately 90% compared to

the unmodulated case. This, at first glance, might seem surprising as after the beam has been switched off the dynamics is subject to the Vlasov–Poisson equations for which a bump-on-tail configuration is unstable. To investigate this in more detail, we consider a plot of the velocity distribution in Figure 3. What we observe is that a velocity plateau for speeds that are roughly between two to five times the thermal velocity develops. There is no bump and thus, as can be shown using the Penrose stability criterion, the distribution is stable. In fact, also in the unmodulated (i.e. constant intensity) case the system is driven to a state that has a velocity plateau. However, in the unmodulated case, the primary physical mechanism is nonlinear saturation induced by the growth of the electric field which forces the plateau. This also results in a state with relatively large spatial variations in the density and consequently large electric energy. On the other hand, the modulated beam, with appropriately chosen frequency and amplitude, drives the system into a state with a velocity plateau that has small density variations and thus also small electric energy.

To analyze this in more detail, we have also plotted the phase space density at different points in time, see the first row for the unmodulated beam and the second row for the sinusoidal beam in Figures 4-6. For the classic bump-on-tail instability the increase in the electric field (initially well described by linear theory) results in an electrostatic potential strong enough to trap particles in the wave (see, e.g.,²⁰). This saturated nonlinear wave then propagates at roughly the beam velocity and can be remarkably stable over long times²¹. Even though the beam is continuously injected into the plasma in the unmodulated case considered here, the observed behavior is very similar. The sinusoidal beam profile, on the other hand, causes different parts of the wave to merge. This starts at relatively early times in the instability and effectively breaks up the overall electrostatic structure, resulting in a spatially more

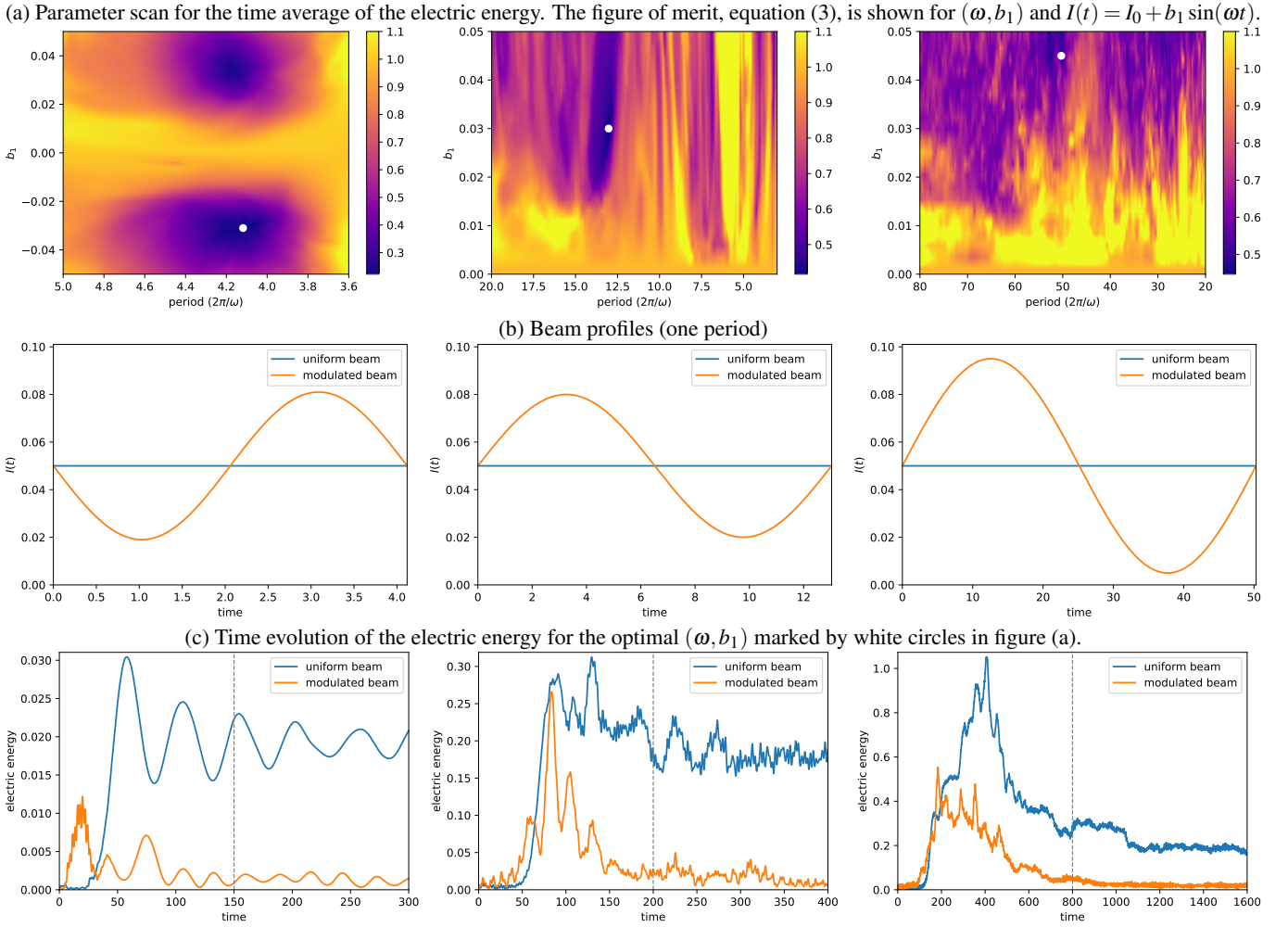


FIG. 2. Numerical results for the sinusoidal beam profile. The dashed gray line indicates the time interval t_f over which the figure of merit is computed.

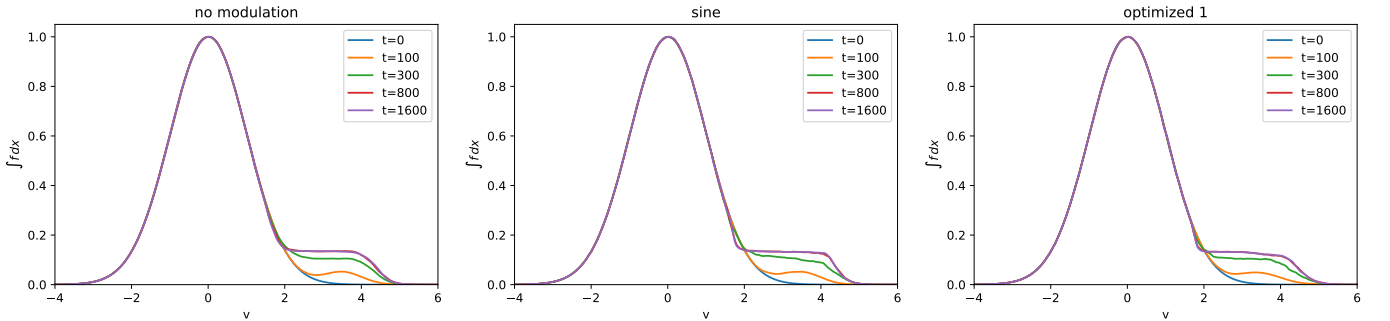


FIG. 3. The spatially averaged distribution function is shown for different times and different beam modulations for the $L = 64\pi$ configuration. For the exact specification of the beam modulation in the middle (sine) and right (optimized 1) we refer to Table I.

homogeneous plasma.

The important observation here is that the driving frequency ω for the sinusoidal beam can be chosen roughly inversely proportional to the system size. Most results that have been obtained in the literature, on the other hand, predict a frequency close to the plasma frequency^{11,13,16}, i.e. independent

of the system size. To understand this, let us consider a simple phenomenological model: the Van der Pol oscillator (as used in¹¹), i.e. a driven oscillator with a quadratic term that models linear exponential growth for small amplitudes and nonlinear saturation for larger amplitudes. In this case, driving the system with the natural oscillation frequency results in suppress-

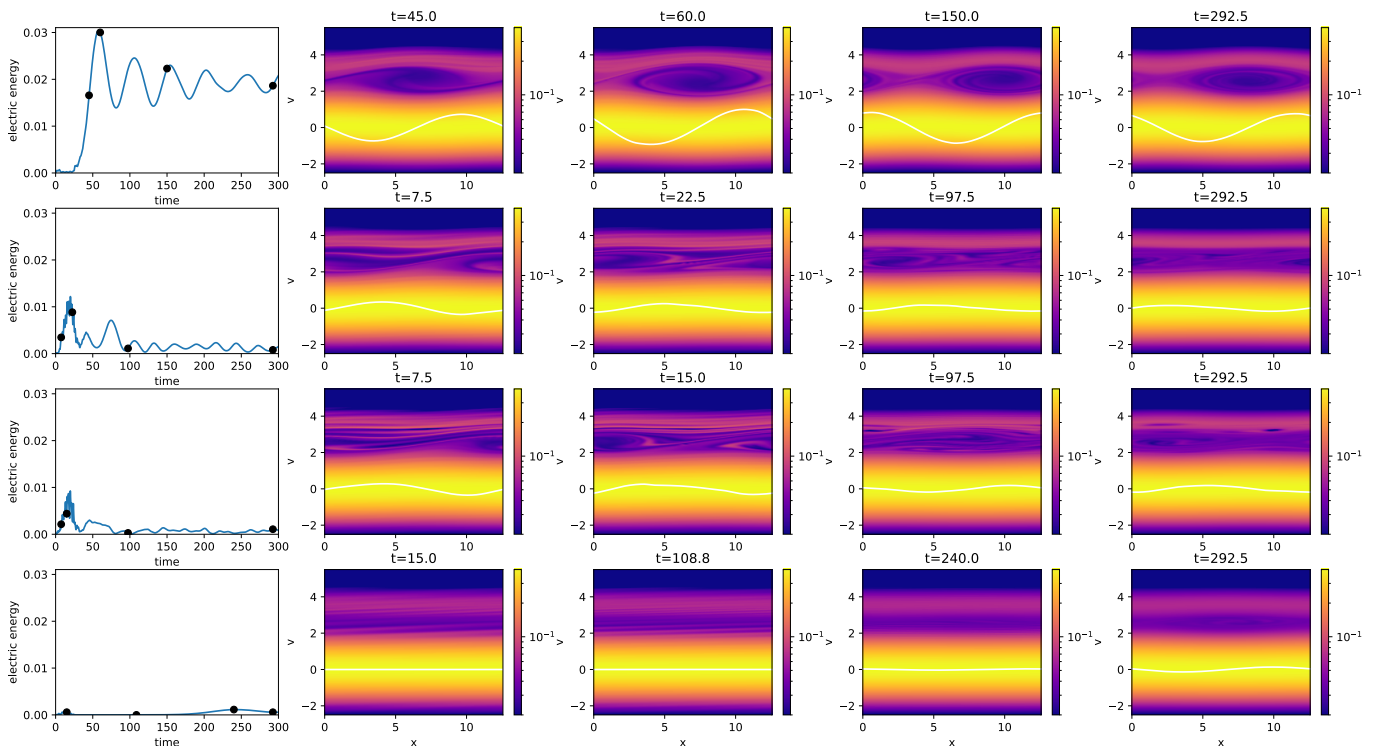


FIG. 4. Plots of the phase space density for the small system size ($L = 4\pi$) at different times in the evolution of the instability are shown. The times chosen are indicated with black dots in the plot of electric energy vs time on the left-hand side of the figure. From top to bottom the following beam profiles are shown: uniform, sine, optimized 1, and optimized 2. All beam profiles are plotted in Figures 7 and a detailed list of the parameters are given in Table I.

sion of the instability. In the present setting this example is most directly related to the smallest domain size ($L = 4\pi$). In this case there is only a single unstable mode. Solving the dispersion relation for the bump-on-tail instability (which obviously neglect time dependent beam propagation effects) gives $\omega_{\text{osc}} \approx 1.45$ which matches well with $\omega \approx 1.53$ as given in Figure 2. Non phenomenological models can be derived. However, they usually rely on decoupling the spatial modes (as Fourier techniques are used). This misses an important effect. Namely, that to excite oscillations with the largest possible wavelength in space, a frequency of $\omega = v_b/L$ is sufficient. In fact, if ω is not an exact multiple of v_b/L multiple modes are excited. This allows for manipulation of the bump-on-tail feature with frequencies that are large compared to the plasma frequency, leading to the observed results. This is immensely useful as it means that for large systems we do not need to modulate the beam at frequencies comparable to the (usually very high) plasma frequency.

IV. RESULTS FOR GENERAL BEAM PROFILES

We now turn our attention to the case of more general beam profiles. That is, our goal is to find $I(t)$, σ , and $v_{ih,b}$ (subject to the constraints outlined in section II), that reduce the figure of merit as much as possible. This can be formulated as an

optimization problem

$$\min_{I(t), \sigma, v_{ih,b}} \int_0^{t_f} \int_0^L \left(E[f_{I, \sigma, v_{ih,b}}](t) \right)^2 dx dt, \quad (4)$$

where $f_{I, \sigma, v_{ih,b}}$ denotes the solution of equation (1) for the specified parameters. The beam intensity is subject to the constraint that $I(t) \geq 0$ and a fixed total intensity $\int_0^{t_b} I(t) dt = I_0 t_b$. However, for such a scheme to be useful in practice, we have to constrain $I(t)$ such that it varies in a reasonable manner. There are many possibilities to do this. We enforce this here by only allowing a couple of Fourier modes. That is, we parameterize $I(t)$ as

$$I(t) = \max \left(I_0 + \sum_{k=1}^{K-1} a_k \cos(k\omega_0 t) + \sum_{k=1}^K b_k \sin(k\omega_0 t), 0 \right).$$

Taking the maximum is necessary because some combination of parameters (a_k, b_k) can result in negative beam intensities, which is clearly unphysical. By taking the maximum with 0, we violate the constraint of fixed total intensity. However, we always have $\int_0^{t_b} I(t) dt > I_0 t_b$ and thus finding such a result in the optimization would indicate that a smaller electric energy with a (slightly) higher beam intensity has been achieved, which is clearly a favorable outcome.

We emphasize that, as Figure 2a already makes clear, the landscape of the optimization problem is quite rough. Thus,

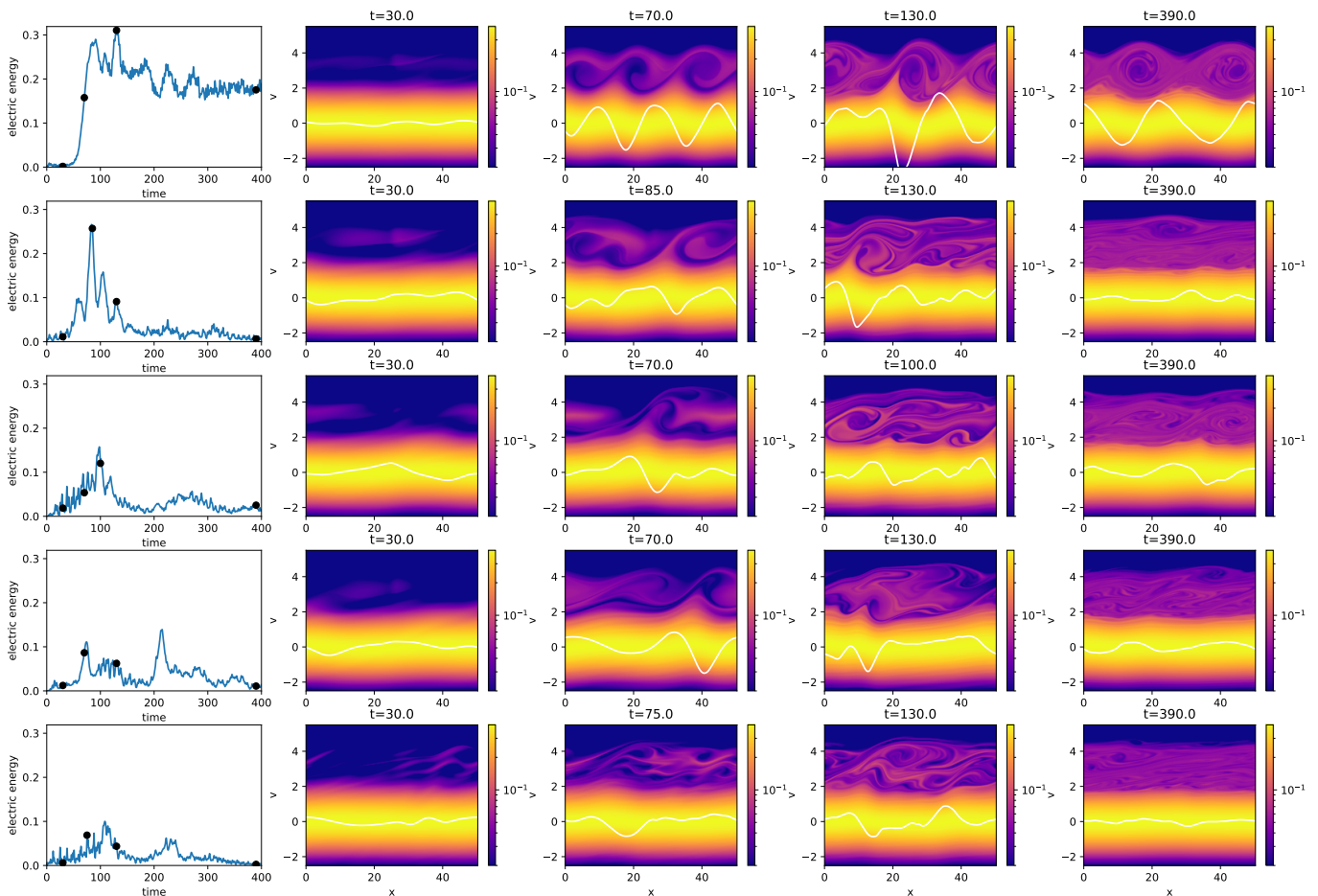


FIG. 5. Plots of the phase space density for the medium system size ($L = 16\pi$) at different times in the evolution of the instability are shown. The times chosen are indicated with black dots in the plot of electric energy vs time on the left-hand side of the figure. From top to bottom the following beam profiles are shown: uniform, sine, optimized 1, optimized 2, and optimized 3. All beam profiles are plotted in Figures 7 and a detailed list of the parameters are given in Table I.

we have a global optimization problem with many local minima and a total of $2K + 2$ parameters. In the following we will present the obtained results. However, some more details on our approach to solve this optimization problem in an efficient way are outlined in section VI.

In Figure 7 we present the best candidates that have been obtained from the numerical optimization and compare them to the sinusoidal beam profile found in the previous section. Note that the global optimization algorithm does not give a unique solution but a number of candidates. We have selected the best (according to the figure of merit) candidates where *optimized 1* only optimizes for the beam profile (but keeps σ fixed) and *optimized 2* simultaneously optimizes the beam profile as well as σ and $v_{rh,b}$. For the intermediate problem size we have also included an optimization run (called *optimized 3* in the plot) with $K = 5$ (in all other configuration $K = 3$ is used). The parameters of all configurations can be found in Table I. For the two larger system sizes we roughly observe a reduction of the severity of the instability by approximately 75-80%, which is a further reduction compared to the

sinusoidal beam profile by approximately a factor of 2. The outlier here is the smallest system size, where the figure of merit decreases by more than 99%. We also see excellent behavior with respect to long time behavior (i.e. after the beam has been switched off). The frequency required to achieve this is, again, roughly inversely proportional to the system size.

We also note that the beam width σ has a relatively minor effect on the result. We have restricted the optimization such that σ is at least 0.2, 0.8, and 3.2 for the small, medium, and large system sizes, respectively. While the optimal solution obtained generally has a value close to this, we have included a candidate with $\sigma \approx 6.26$ (*optimized 2* for the large problem size) to demonstrate that even for larger beam widths the achieved figure of merit only deteriorates slightly.

We further study the velocity dependence of a optimized solution in Figure 3 on the right. As expected the solution is driven to a state with a plateau in the velocity distribution. In fact, we observe that the dynamics produces almost no bump-on-tail feature in this case. This can be seen in more detail by the phase space plots in Figures 4-6, where we observe

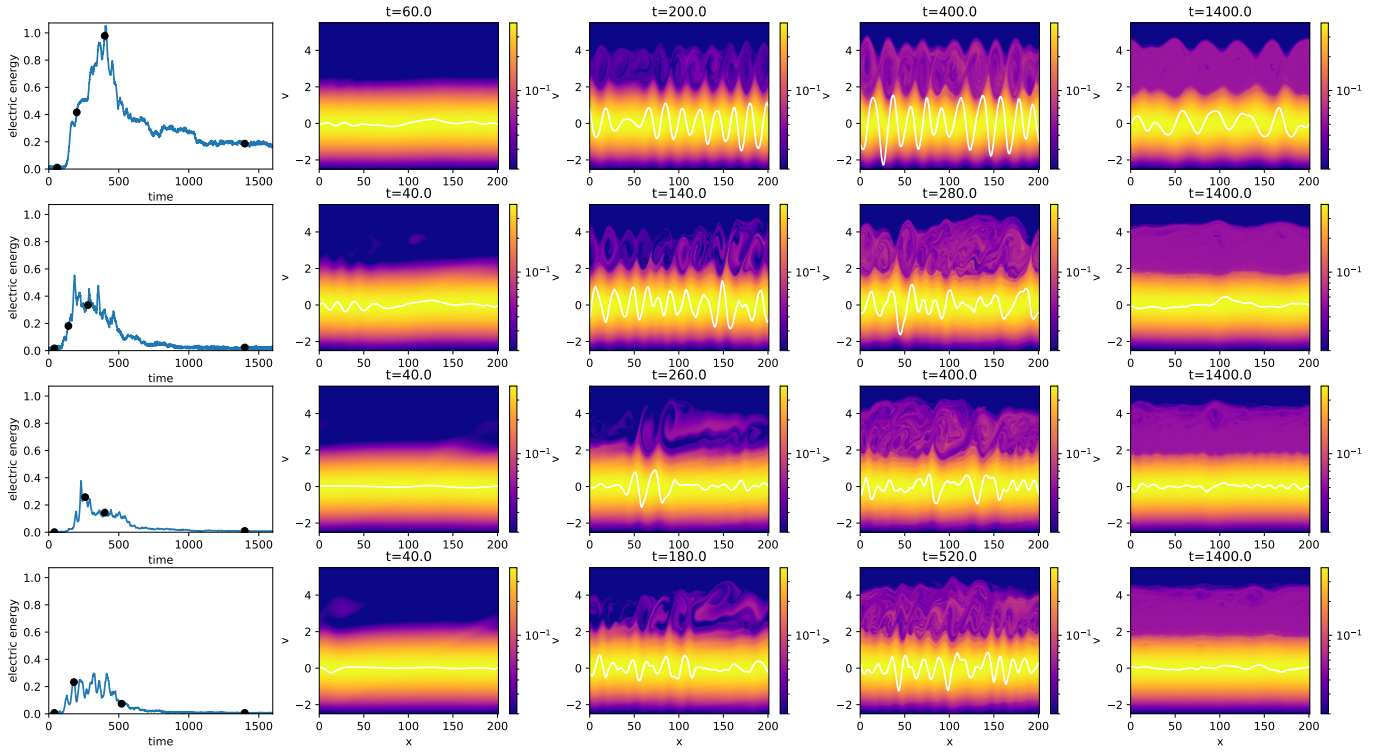


FIG. 6. Plots of the phase space density for the large system size ($L = 64\pi$) at different times in the evolution of the instability are shown. The times chosen are indicated with black dots in the plot of electric energy vs time on the left-hand side of the figure. From top to bottom the following beam profiles are shown: uniform, sine, optimized 1, and optimized 2. All beam profiles are plotted in Figures 7 and a detailed list of the parameters are given in Table I.

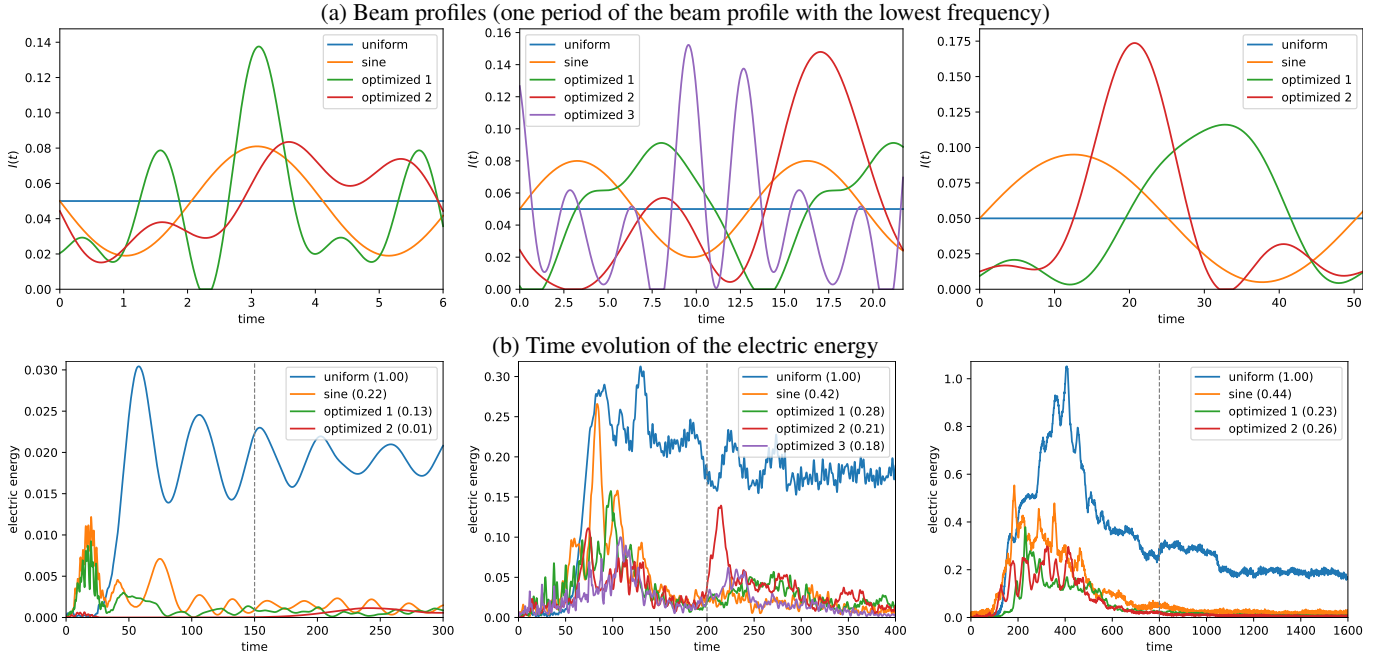


FIG. 7. Comparison of the beam profiles found by numerical optimization (denoted by optimized 1, optimized 2, and optimized 3; the parameters can be found in Table I) with the optimal sinusoidal beam profiles from section III. The figure of merit is shown in parentheses in the legend and the dashed gray line indicates the time interval t_f over which the figure of merit is computed.

that the beam profiles found by optimization are even more effective in merging the parts of the electrostatic waves and thus reducing the amplitude of the instability.

V. ROBUSTNESS OF THE BEAM PROFILES TO PERTURBATION

A control scheme would not be very useful in practice if even minor perturbations, e.g. due to imperfection in the control of the beam, would be sufficient to negate its effect. This is what we will study in this section. We run the simulations as before, but with the parameters in Table I perturbed by multiplying them with uniformly distributed random numbers in the range $[1 - \varepsilon, 1 + \varepsilon]$. This gives a modified beam profile and the corresponding results are shown in Figure 8. We observe that the figure of merit is remarkably robust at least for perturbations of up to 5% in all parameters. The only outlier is the optimized 1 beam profile for the intermediate system size, which relatively quickly deteriorates to the level of the sinusoidal beam profile. Thus, different beam profiles can behave differently with respect to such perturbations. In principle, one could also perform the optimization taking this into account. For example, by penalizing beam profiles that are not robust. However, with one exception all beam profiles found using the optimization algorithm (that only takes the figure of merit into account) turned out to be robust.

VI. METHODOLOGY

Finding the parameters $(\omega_0, a_k, b_k, \sigma, v_{th,b})$ of the optimization problem given in equation (4) requires a global optimization algorithm in order to avoid being stuck in local minima. We use a modification of the genetic optimization algorithm found in `scipy.optimize.differential_evolution`²². The genetic optimization algorithm can be setup such that in each generation the figure of merit (or fitness) for all candidate solutions (which are sets of parameters that determine the beam profiles) are evaluated at the same time. This is beneficial from a computational point of view, as calling individual runs of a one-dimensional Vlasov–Poisson solver has a relatively large overhead due to the small problem size. In order to avoid this we have developed a C++ code that solves equation (1) in a batched manner (i.e. multiple beam profiles at the same time). The code uses the Kokkos performance portability programming ecosystem²³ and can thus make use of modern computing systems equipped with graphic processing units (GPUs).

In the optimization algorithm the simulations are run with 512 grid points in the spatial direction, 256 grid points in the velocity direction, and a time step size $\Delta t = 0.02$. A splitting based semi-Lagrangian scheme with 9th order Lagrange interpolation is employed. However, in order to make sure that all results obtained from the optimization algorithm are independent of the numerical parameters used, all the data required for the plots in this paper have been run with increased resolution (1024 grid points in the spatial, 512 grid points in the

velocity direction, and a time step size $\Delta t = 0.01$).

VII. DISCUSSION

In this work, we have investigated how much control can be achieved by modulating the intensity of a beam in an electrostatic beam-plasma instability. We have found beam profiles that drastically reduce the severity of the instability. In all configurations studied here, control schemes have been obtained that reduce the time averaged electric energy (a measure of the severity of the instability) by at least 75% compared to its original value.

A pertinent question is whether such or a related control scheme can be applied in practice. In that regard, it is encouraging that, as we have demonstrated, a significant reduction in the severity of the instability can be observed with a beam modulation that

- requires no feedback (i.e. measurements) during the evolution of the instability. Control without feedback is possible since the modulation of the beam (i.e. how the system is driven) has a significant influence on the velocity distribution. In fact, the bump-on-tail feature can largely be avoided for the optimized beam profiles and even for sinusoidally modulated beams is significantly reduced;
- the frequency at which we need to modulate the beam scales favorably with system size. This is important in practice as the frequency of the beam determines how fast the control (here the beam intensity) has to be actuated and consequently how easy it is to implement such a scheme. This is, in particular, favorable as in many systems of interest where beam heating is employed the size of a plasma system can be many thousands of Debye lengths;
- is able to drive the system to a state that remain stable after the beam has been switched off. This state has a plateau in velocity space and almost uniform density in space, which implies that little kinetic energy from the beam is transferred to the field;
- is robust with respect to perturbations in the beam profile. That is, imperfections in the beam profile (as are unavoidable in practice) do not significantly diminish the performance of the control scheme.
- does not require a tight focusing of the beam. In fact, we found that the beam width (for a beam width of up to 3% of the domain size) has only a small influence on the effectiveness of the control.

We emphasize that our control scheme relies on the time evolution of the bump-on-tail feature to be effective. This is different from the situation in, e.g.¹³, where two streams are already established and are then subsequently modulated by applying an external electric field. We take the viewpoint that, at

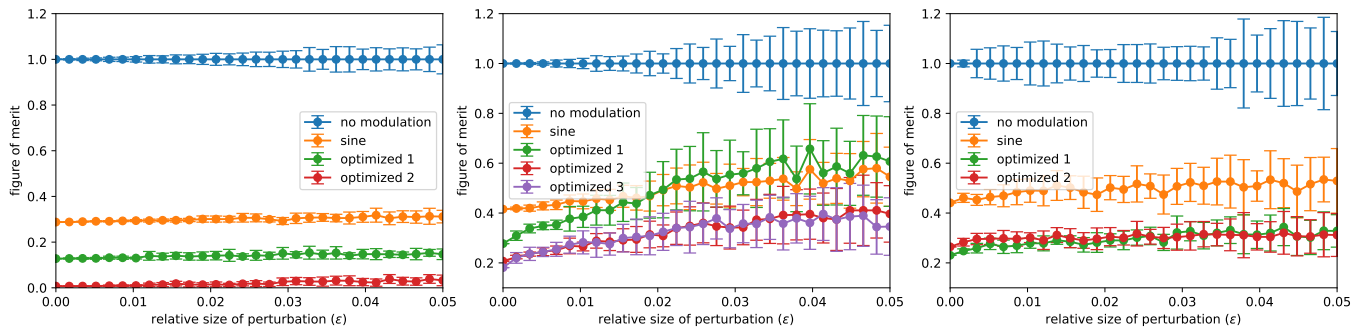


FIG. 8. The figure of merit as a function of the relative size of the perturbation ϵ in the parameters that determine the beam profile is shown. For each ϵ we consider 20 random perturbations and their average figure of merit as well as the standard deviation is shown. Since the perturbation also changes the figure of merit for the case with an unmodulated beam, we have normalized all plots to the corresponding average value for the unmodulated beam at that size of the perturbation.

least in beam heating applications, assuming an already established bump-on-tail feature is more a modeling artifact often required to make theoretical progress than a reasonable experimental setup.

Let us also point out that we do not model the actual heating (i.e. the thermalization of the velocity distribution by collisions) here. In the spatially homogeneous case, it can be easily inferred that the system relaxes to a Maxwellian with increased temperature after the beam has been switched off. The numerical simulation show that a small degree of spatial variation remains. Nevertheless, since the state obtained after the beam has been switched off is stable, we expect the same result to hold true. We consider this as future work.

For the present study we have used a simple one-dimensional model with stationary ions. In many applications of practical relevance more faithful models are required that are much more complicated and more challenging numerically (e.g. due to the timescale separation between ions and electrons, up to six dimensions in phase space, the beam consisting of both electrons and ions, etc.). This presents a significant challenge as in order to solve the global optimization problem many simulations have to be conducted. Thus, in order to find good beam profiles in such a situation would most likely require either some type of complexity reduction techniques/reduced models or large-scale supercomputers. We also note that in more realistic problems there are many more parameters that could be part of the optimization algorithm (e.g. the angle at which a beam penetrates into the plasma), which conceivable could help in reducing the severity of the instability.

ACKNOWLEDGEMENTS

We would like to thank the anonymous reviewers for their insightful comments that helped to improve the paper. We would also like to thank Qin Li (University of Wisconsin, Madison), Li Wang (University of Minnesota) and Yunan Yang (Cornell University) for fruitful discussions on optimization algorithms and plasma stability.

- ¹J. Denavit, "Simulations of the single-mode, bump-on-tail instability," *Phys. Fluids* **28**, 2773–2777 (1985).
- ²M. Yamagiwa, T. Takizuka, and Y. Kishimoto, "Effective ion tail formation by beam and ion cyclotron heating," *Nucl. Fusion* **27**, 1773–1784 (1987).
- ³N. Carlevaro, M. Falessi, G. Montani, and F. Zonca, "Nonlinear physics and energetic particle transport features of the beam-plasma instability," *J. Plasma Phys.* **81** (2015), 10.1017/s0022377815001002.
- ⁴M. V. Zeeland, L. Bardoczi, J. Gonzalez-Martin, W. Heidbrink, M. Podesta, M. Austin, C. Collins, X. Du, V. Duarte, M. Garcia-Munoz, S. Munaretto, K. Thome, Y. Todo, and X. Wang, "Beam modulation and bump-on-tail effects on Alfvén eigenmode stability in DIII-D," *Nuclear Fusion* **61**, 066028 (2021).
- ⁵E. Speth, "Neutral beam heating of fusion plasmas," *Rep. Progr. Phys.* **52**, 57–121 (1989).
- ⁶B. Breizman, P. Aleynikov, E. Hollmann, and M. Lehnen, "Physics of runaway electrons in tokamaks," *Nucl. Fusion* **59**, 083001 (2019).
- ⁷C. Liu, D. Brennan, A. Lvovskiy, C. Paz-Soldan, E. Fredrickson, and A. Bhattacharjee, "Compressional Alfvén eigenmodes excited by runaway electrons," *Nucl. Fusion* **61**, 036011 (2021).
- ⁸D. Jing, L. Chang, X. Yang, Y. Xia, J.-H. Zhang, H.-S. Zhou, and G.-N. Luo, "Exploration on the Possible Bump-on-Tail Instability in VASIMR," *Space: Science & Technology* **4** (2024), 10.34133/space.0107.
- ⁹M. Burger, R. Pinnau, C. Totzeck, O. Tse, and A. Roth, "Instantaneous control of interacting particle systems in the mean-field limit," *J. Comput. Phys.* **405**, 109181 (2020).
- ¹⁰G. Albi, G. Dimarco, F. Ferrarese, and L. Pareschi, "Instantaneous control strategies for magnetically confined fusion plasma," *arXiv:2403.16254* (2024), 10.48550/ARXIV.2403.16254.
- ¹¹Y. Nakamura, "Suppression of Two-Stream Instability by Beam Modulation," *Journal of the Physical Society of Japan* **28**, 1315–1321 (1970).
- ¹²O. Fukumasa and R. Itatani, "Numerical simulation on the nonlinear interaction between a modulated electron beam and a plasma," *Plasma Physics* **24**, 1219–1242 (1982).
- ¹³H. Qin and R. Davidson, "Two-stream instability with time-dependent drift velocity," *Phys. Plasmas* **21** (2014), 10.1063/1.4885076.
- ¹⁴S. Kawata, T. Karino, and Y. J. Gu, "Dynamic stabilization of plasma instability," *High Power Laser Sci. Eng.* **7** (2018), 10.1017/hpl.2018.61.
- ¹⁵L. Einkemmer, Q. Li, L. Wang, and Y. Yang, "Suppressing instability in a Vlasov–Poisson system by an external electric field through constrained optimization," *J. Comput. Phys.* **498**, 112662 (2024).
- ¹⁶L. Einkemmer, Q. Li, C. Mouhot, and Y. Yue, "Control of Instability in a Vlasov–Poisson System Through an External Electric Field," *arXiv:2407.15008* (2024), 10.48550/ARXIV.2407.15008.
- ¹⁷F. F. Chen, *Introduction to Plasma Physics and Controlled Fusion* (Springer, 2016).
- ¹⁸D. G. Swanson, *Plasma Waves* (CRC Press, 2020).
- ¹⁹O. Penrose, "Electrostatic Instabilities of a Uniform Non-Maxwellian Plasma," *Physics of Fluids* **3**, 258–265 (1960).
- ²⁰J. Tennyson, J. Meiss, and P. Morrison, "Self-consistent chaos in the beam-plasma instability," *Physica D* **71**, 1–17 (1994).

	$L = 4\pi$	$L = 16\pi$	$L = 64\pi$
sine	$\omega_0 = 1.5258$ $\sigma = 0.2$ $v_{th,b} = 0.5$ $I_0 = 0.05$ $b_1 = -0.031$	$\omega_0 = 0.48221$ $\sigma = 0.8$ $v_{th,b} = 0.5$ $I_0 = 0.05$ $b_1 = 0.03$	$\omega_0 = 0.12491$ $\sigma = 3.2$ $v_{th,b} = 0.5$ $I_0 = 0.05$ $b_1 = 0.045$
optimized 1	$\omega_0 = 1.5515$ $\sigma = 0.2$ $v_{th,b} = 0.5$ $I_0 = 0.05$ $b_1 = -0.026653$ $a_1 = -0.00091327$ $b_2 = -0.02506$ $a_2 = -0.028601$ $b_3 = 0.029389$	$\omega_0 = 0.47789$ $\sigma = 0.8$ $v_{th,b} = 0.5$ $I_0 = 0.05$ $b_1 = -0.015525$ $a_1 = -0.037118$ $b_2 = -0.00095985$ $a_2 = -0.010956$ $b_3 = -0.0065273$	$\omega_0 = 0.12455$ $\sigma = 3.2$ $v_{th,b} = 0.59837$ $I_0 = 0.05$ $b_1 = -0.035227$ $a_1 = -0.042398$ $b_2 = 0.016937$ $a_2 = 0.0017211$ $b_3 = 0.0094516$
optimized 2	$\omega_0 = 1.0472$ $\sigma = 1$ $v_{th,b} = 0.6$ $I_0 = 0.05$ $b_1 = -0.024724$ $a_1 = -0.007559$ $b_2 = -0.001239$ $a_2 = 0.0019077$ $b_3 = -0.014125$	$\omega_0 = 0.28944$ $\sigma = 0.8$ $v_{th,b} = 0.6$ $I_0 = 0.05$ $b_1 = -0.045485$ $a_1 = 0.0046448$ $b_2 = -0.031921$ $a_2 = -0.030133$ $b_3 = 0.014797$	$\omega_0 = 0.12278$ $\sigma = 6.262$ $v_{th,b} = 0.59782$ $I_0 = 0.05$ $b_1 = 0.035498$ $a_1 = -0.047241$ $b_2 = -0.042762$ $a_2 = 0.0097479$ $b_3 = 0.021815$
optimized 3		$\omega_0 = 0.48407$ $\sigma = 0.80088$ $v_{th,b} = 0.59999$ $I_0 = 0.05$ $b_1 = -0.020504$ $a_1 = 0.023424$ $b_2 = -0.00080311$ $a_2 = -0.0064016$ $b_3 = 0.011956$ $a_3 = 0.014704$ $b_4 = -0.022388$ $a_4 = 0.044865$ $b_5 = -0.013898$	

TABLE I. The parameters of the optimized beam profiles that are discussed in sections III and IV are listed.

²¹N. Balmforth, “BGK states from the bump-on-tail instability,” *Commun. Nonlinear Sci.* **17**, 1989–1997 (2012).

²²P. Virtanen, R. Gommers, T. Oliphant, M. Haberland, T. Reddy, D. Cournapeau, E. Burovski, P. Peterson, W. Weckesser, J. Bright, *et al.*, “SciPy 1.0: Fundamental Algorithms for Scientific Computing in Python,” *Nature*

Methods **17**, 261–272 (2020).

²³C. Trott, D. Lebrun-Grandié, D. Arndt, J. Ciesko, V. Dang, N. Ellingwood, R. Gayatri, E. Harvey, D. Hollman, D. Ibanez, *et al.*, “Kokkos 3: Programming model extensions for the exascale era,” *IEEE Transactions on Parallel and Distributed Systems* **33**, 805–817 (2022).